

# Ab-initio simulation of excited-state potential energy surfaces with transferable deep quantum Monte Carlo

Zeno Schätzle<sup>1†</sup>, P. Bernát Szabó<sup>1†</sup>, Alice Cuzzocrea<sup>1</sup>,  
Frank Noé<sup>1,2,3,4\*</sup>

<sup>1</sup>Department of Mathematics and Computer Science, FU Berlin,  
Arnimallee 6, Berlin, 14195, Berlin, Germany.

<sup>2</sup>Department of Physics, FU Berlin, Arnimallee 14, Berlin, 14195,  
Berlin, Germany.

<sup>3</sup>AI for Science, Microsoft Research, Karl-Liebknecht Str. 32, Berlin,  
10178, Berlin, Germany.

<sup>4</sup>Department of Chemistry, Rice University, Street, Huston, 77005,  
Texas, United States.

\*Corresponding author(s). E-mail(s): [frank.noe@fu-berlin.de](mailto:frank.noe@fu-berlin.de);

†These authors contributed equally to this work.

## Abstract

The accurate quantum chemical calculation of excited states is a challenging task, often requiring computationally demanding methods. When entire ground and excited potential energy surfaces (PESs) are desired, e.g., to predict the interaction of light excitation and structural changes, one is often forced to use cheaper computational methods at the cost of reduced accuracy. Here we introduce a novel method for the geometrically transferable optimization of neural network wave functions that leverages weight sharing and dynamical ordering of electronic states. Our method enables the efficient prediction of ground and excited-state PESs and their intersections at the highest accuracy, demonstrating up to two orders of magnitude cost reduction compared to single-point calculations. We validate our approach on three challenging excited-state PESs, including ethylene, the carbon dimer, and the methylenimmonium cation, indicating that transferable deep-learning QMC can pave the way towards highly accurate simulation of excited-state dynamics.

**Keywords:** Excited States, Quantum Monte Carlo, Deep Learning, Parameter Sharing

Photochemistry plays a fundamental role in biological systems, driving essential processes such as vision, photosynthesis, and molecular photoprotection [1–3]. Light-driven phenomena are also key to technological advancements, ranging from material design and chemical processing [4, 5] to biomedical technologies such as molecular motors and photo-controlled drug delivery [6, 7].

Despite the critical importance of these processes, their theoretical study is hindered by the need for accurate *ab-initio* descriptions of electronic excited states. Most quantum chemistry methods have been developed for the calculation of electronic ground states and their extensions to excited states are either limited or highly expensive and often require expert knowledge [8, 9]. These problems are further amplified when targeting a coherent description of excited state potential energy surfaces (PESs), which are the key ingredient to simulating the photodynamics of molecules [10]. Time-dependent density functional theory is widely used for excited-state characterization but struggles with delocalized excitations, conical intersections, high-energy states, multi-electron processes, and charge transfer [11, 12]. Similarly, excited-state extensions of coupled cluster methods, which rely on a single reference determinant, become unreliable in systems with strong multi-reference character [13]. On the other hand, most multi-reference methods require the definition of an active space, a process that often relies on chemical intuition to select relevant orbitals and becomes increasingly challenging when considering structural flexibility, i.e. in dynamical simulations [14]. Even if sophisticated automatic tools are used to obtain appropriate active spaces [14, 15], accurately describing dynamic correlation often necessitates the use of multi-reference coupled cluster or (semi-stochastic) configuration interaction (CI) methods. However, these approaches remain less established than their single-reference counterparts and exhibit steep computational scaling with system size [16].

Variational quantum Monte Carlo (VMC) offers a promising alternative to traditional methods, given its black-box nature, favorable scaling with system size, and flexibility to address virtually any electronic structure problem [17–19]. Neural network based VMC [20–22] has recently been shown to yield high accuracy in challenging excited-state problems, including conical intersections and double excitations. Despite this success, the simulation of excited-state PESs remains costly due to the need of performing large numbers of independent single-point calculations. At the same time, sharing neural network wave function parameters across molecular geometries (geometric transferability) [23, 24] was shown to be both accurate and computationally efficient in simulating ground state PESs and proved beneficial for generalizing across molecules [25–27] as well as spin lattice Hamiltonians [28]. Extending geometric transferability of neural network wave functions to excited state calculations promises a wide range of benefits, including reduced computational costs, improved error cancellation, as well as more stable optimization processes. Such an approach could provide unparalleled *ab-initio* access to all electronic properties of even the most challenging excited states at a systematically refinable accuracy.

In this work, a method for the transferable VMC optimization of neural network wave functions for excited-state PESs is presented. Exploiting similarities of wave functions across molecular geometries, the efficiency of computing excited-state PESs is increased significantly over single-point simulations, with a speedup of close to

two orders of magnitude being demonstrated. Further improvements are attained by introducing parameter sharing between electronic states and a dynamic state ordering mechanism for the orthogonalization of states based on the per-geometry energy. The method yields a coherent *ab-initio* description of excited-state PESs with full access to electronic properties, which we demonstrate on three challenging applications – the ground and singlet excited states of the ethylene torsion and pyramidalization PESs, the eight lowest-lying states of the carbon dimer dissociation, and the two-dimensional excited state PESs of the three lowest singlet states of the methylenimmonium cation.

## Results

### Transferable *ab-initio* optimization of excited states

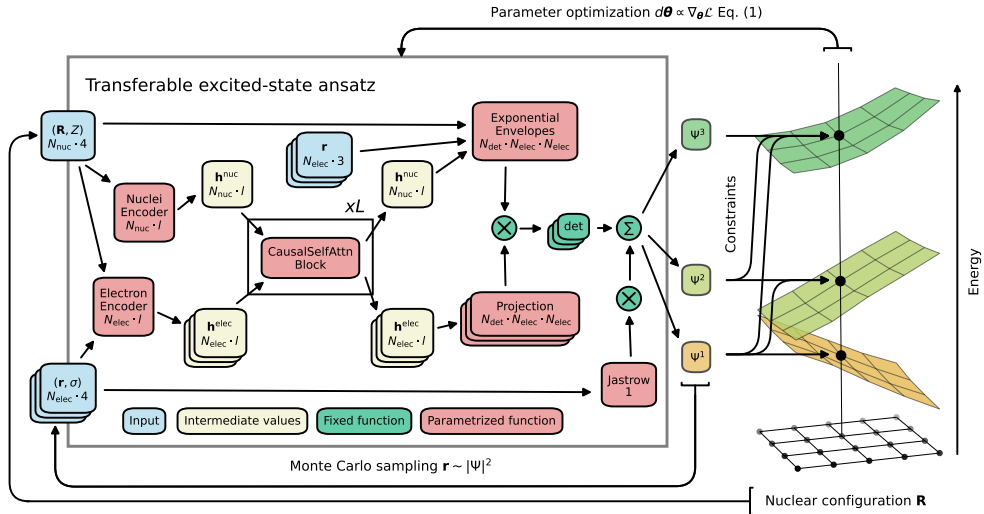


**Fig. 1 Neural network architecture for the transferable excited-state wave function with orthogonality constraints.** Diagram of the transferable wave function. Nuclear positions inform the electron representations in the CAUSALSELFATTN block, introducing an explicit dependency on the molecular configuration. If parameters are shared between states, the same ELECTRON ENCODER, NUCLEI ENCODER and CAUSALSELFATTN block are applied for each batch of electron coordinates, respectively. The orthogonality of the states is implemented by ordering wave functions based on energy and applying a directional overlap penalty (1).

In traditional quantum chemistry, calculating excited-state PESs involves the costly simulation of multiple wave functions for a large number of molecular geometries. Taking advantage of similarities between such wave functions and leveraging the high expressivity of neural network ansatzes, we introduce a method that generalizes across molecular configurations as well as electronic excited states, achieving a balanced description of excited-state PESs at a much reduced cost. The framework

combines multiple components, which we condensed in a loss function for variational Monte Carlo optimization:

$$\mathcal{L}(\underbrace{\theta_1, \dots, \theta_{N_s}}_{\text{shared params}}, \theta^s) = \sum_{\mathbf{R} \in \mathfrak{R}} \underbrace{\sum_i^{N_s}}_{\text{geometry transfer}} \left[ \underbrace{\langle \hat{H} \rangle_{\mathbf{R}}^i}_{\text{energy expectation}} + \beta \underbrace{\langle \hat{S}^2 \rangle_{\mathbf{R}}^i}_{\text{spin penalty}} + \underbrace{\sum_j^{E_{\mathbf{R}}^i > E_{\mathbf{R}}^j} \alpha_{ij} \langle \Psi^i | \bar{\Psi}^j \rangle_{\mathbf{R}}^2}_{\text{dynamic overlap penalty}} \right]. \quad (1)$$

The loss comprises the molecular energy expectation value  $\langle \hat{H} \rangle$ , and the spin-penalty  $\langle \hat{S}^2 \rangle$  [21, 29] for each electronic state  $i$  and configuration  $\mathbf{R}$ . The parameters  $\theta_i$ , one for each of the  $N_s$  states, are optimized simultaneously across a dataset of molecular geometries  $\mathfrak{R}$ , constituting in a significant advancement over the conventional independent treatment [20, 21, 30] in terms of convergence speed and accuracy. Additionally, partial sharing of parameters  $\theta^s$  between different states leads to improved error cancellation (see Sec. 1.5) increasing the accuracy in relative energy.

While previous penalty-based QMC algorithms enabled the computation of multiple excited states via an overlap penalty term between states with a fixed order, the last term of (1) orders states dynamically based on the per-geometry energy  $E_{\mathbf{R}}$  (further details in Sec. 1.3). This enhances the robustness of our method in the presence of level crossings and conical intersections – crucial albeit challenging points for quantum chemistry – promoting the continuity of the ansatzes at points where the energy ordering of the states changes. Notably, due to the regularization properties and improved convergence of the transferable training, the simulation of excited state PESs is further simplified by eliminating the need for supervised pretraining on external quantum chemistry methods. Additionally, incorporating an explicit parametric dependence of the ansatz on nuclear positions further increases expressivity and promotes stable convergence. Concretely, the self-attention block  $\text{SelfAttn}(\mathbf{h}^{\text{elec}})$  of the Psiformer [31] is extended by considering both nuclear and electronic nodes

$$\text{CausalSelfAttn}(\text{Concat}(\mathbf{h}^{\text{nuc}}, \mathbf{h}^{\text{elec}})), \quad (2)$$

with causal attention preventing information from flowing from electrons to nuclei. After applying  $L$  layers of self-attention, the final electron representations  $\mathbf{h}^{\text{elec}}$  are projected to give many-body orbitals and nuclei representations  $\mathbf{h}^{\text{nuc}}$  are used to predict parameters of the orbital envelopes. The architecture of the ansatz is depicted on Fig. 1 and further discussed in Sec. 1.4.

In the following, we demonstrate the benefits of these methodological advancements on several challenging excited-state PESs. Our results are compared to state-of-the-art multi-reference quantum chemistry methods and single-point deep-learning QMC simulations. As a quantitative measure of accuracy, we propose the mean absolute error (MAE) of relative energies, computed between target and reference results after shifting the latter such that their mean energies across all geometries and all states are aligned.

## Unified description of excited state processes

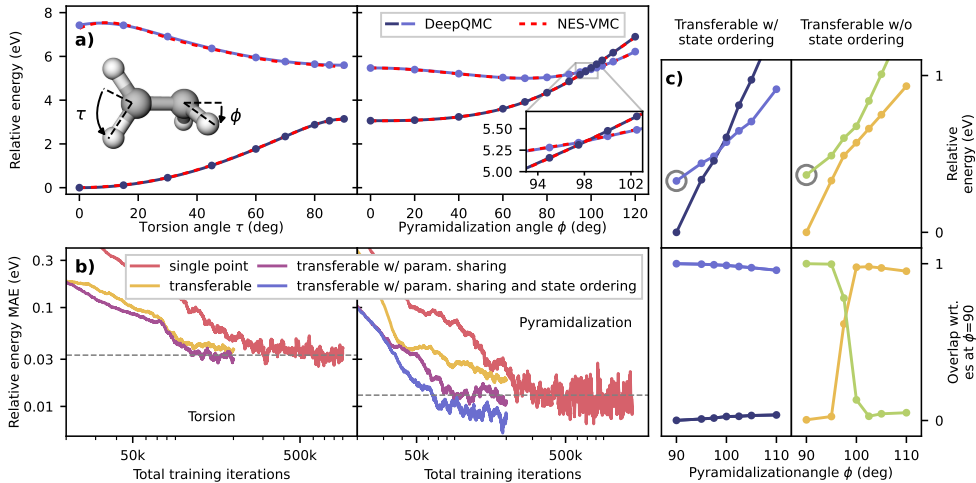


**Fig. 2** Lowest-lying singlet PESs for ethylene relaxation. Simulation of the ground and first singlet excited state of ethylene along the torsion around the C–C bond and pyramidalization of a CH<sub>2</sub> group. **a)** Relative energy with respect to the equilibrium geometry. DeepQMC results for transferable optimization with parameter sharing and dynamic state ordering are presented alongside highly accurate single-point NES-VMC simulations [30]. Sampling errors are smaller than the marker size. **b)** Convergence of the DeepQMC MAEs to NES-VMC results in relative energy. Different variants of transferable DeepQMC optimization are compared to single-point calculations performed in earlier work [21]. The horizontal axis indicates the total cumulative iterations across all geometries of the torsion and pyramidalization PES, respectively. The dashed horizontal line gives the accuracy of evaluating the final single-point wave functions. **c)** Relative energies with respect to  $\phi = 90^\circ$  around the conical intersection (top two panels) and intermolecular overlaps (Eq.11, bottom two panels) for transferable DeepQMC runs with parameter sharing and dynamic state ordering and without parameter sharing and fixed ordering.

Ethylene serves as a minimal model system for photoisomerization processes and internal energy conversion and its excited-state PES has been studied extensively [32, 33]. After photo-excitation to the first singlet excited state, ethylene undergoes a torsion around the carbon-carbon bond and a pyramidalization of one of the CH<sub>2</sub> units, leading to a conical intersection from which the system relaxes back to the ground state equilibrium geometry. Computationally modeling the non-radiative relaxation pathway is challenging due to strong electronic correlation in the excited state, increasing multi-reference character upon approaching the conical intersection, and the existence of intersystem crossings. It has been shown that single-reference methods such as SR-CI qualitatively fail at describing several features of the ethylene PES [32–34]. Deep-learning QMC, on the other hand, does not suffer from these limitations [22, 35] and previous, single-point applications of excited state deep-learning QMC methods have modeled the PESs of ethylene with high accuracy [20, 21, 30].

In this work, two transferable DeepQMC optimizations are run for the 1D PESs along the torsion (9 geometries) and pyramidalization (14 geometries) of ethylene [33]. The spin penalty (1) is utilized to target singlet states only. The results of the transferable optimization with parameter sharing and dynamic state ordering displayed in Fig. 2, are in excellent agreement with the single-point natural excited state (NES) QMC reference [30]. After a total of 200k training iterations evenly split across all geometries, we obtain a MAE for the relative energies of 29.4(1) meV along the torsion PES, and 4.7(7) meV along the pyramidalization PES. This improves over previously obtained, single-point, penalty-based DeepQMC results [21] of 33.8(3) meV and 13.1(3) meV, while using about five times fewer computational resources and without employing supervised pretraining with respect to CASSCF baselines. The location of the conical intersection of the pyramidalization PES ( $98.5^\circ$ ) is excellently reproduced, while due to the dynamic ordering of the states the ansatzes are continuous across the conical intersection.

The beneficial effects of dynamic state ordering and parameter sharing are highlighted in Fig. 2b, comparing the convergence of the relative energy MAEs during optimization with and without parameter sharing and dynamic state ordering. First, dynamic state ordering facilitates convergence in the presence of a conical intersection, reaching lower errors faster, than other transferable calculations on the pyramidalization PES. Second, sharing the parameters of the main electron-nucleus transformer across the two ansatzes leads to improved convergence of the MAE of relative energies compared to independent transferable wave functions on both PESs. The effect of the dynamic state ordering is furthermore illustrated in Fig. 2c, where energies and intermolecular overlaps at the conical intersection are shown. While the runs with the option turned on are continuous through the crossing and intermolecular overlaps stay close to one within a state and close to zero with respect to the second state, runs without dynamic state ordering display a discontinuity at the conical intersections, where the intermolecular overlaps indicate a flip of the states.

## Efficiently simulating challenging electronic structures

Computing the numerous low-lying electronic states of the dissociation of the carbon dimer constitutes a formidable challenge to quantum chemistry methods [36, 37]. The difficulty lies in the simultaneous presence of strong static and dynamic correlation [38], giving rise to a number of exotic electronic properties such as charge-transfer type bonding [39], and the presence of low-lying doubly excited states [40].

The benefits of optimizing excited state deep-learning QMC ansatzes jointly across molecular geometries are showcased by modeling the lowest-lying eight states of the carbon dimer simultaneously for ten nuclear separations ranging from 1.0 to 1.9 Å. Utilizing the spin penalty term in the loss function (1), the four singlet and four triplet states can be treated separately. The parameters of the main electron-nucleus transformer are shared across the four electronic states in each simulation. The resulting PESs are shown on Fig. 3a, along with reference values obtained with the semi-stochastic heat bath configuration interaction (SHCI) [36] method. It is clear that joint DeepQMC optimization is capable of modeling all eight states, along the entire range of bond lengths. The convergence of the MAE of relative energies during the

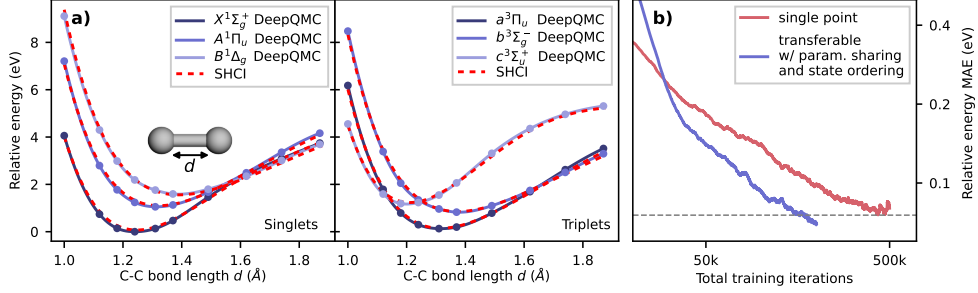


**Fig. 3 Carbon dimer dissociation curves along the lowest-lying eight electronic states.** Transferable DeepQMC ansatzes were trained jointly across ten geometries, with bond lengths ranging from 1.0 to 1.9 Å. Semistochastic heat-bath configuration interaction calculations in quintuple- $\zeta$  basis, extrapolated to the full configuration interaction limit are used as reference [36]. **a)**: The final relative energies obtained with transferable DeepQMC, for the lowest-lying four singlet and four triplet states of the carbon dimer. Both DeepQMC and reference curves were smoothed by cubic interpolation. **b)**: Convergence of the mean absolute error of relative energies between the eight lowest-lying states of the carbon dimer. Geometrically transferable optimization is compared with single-point training performed in earlier work [21]. The horizontal axis indicates the total cumulative iterations across all geometries. The dashed horizontal line marks the evaluated final accuracy of the single-point simulations.

training process is plotted on Fig. 3b, for single-point [21], and transferable DeepQMC optimizations. The final MAEs of the two setups are similar, being 75(2) meV for single-point, and 69(1) meV for transferable optimization. However, joint training offers large cost savings, converging to this accuracy significantly faster: it reaches the final MAE of the single-point calculation in about three times fewer iterations. This is all the more remarkable as unlike the single-point run, transferable optimization was not preceded by supervised pretraining. It’s worth emphasizing that the above results pertain to the accuracy of relative energies, as opposed to the absolute energy of each point along the PESs. While the former is vastly more important in practice, we note that the model trained jointly for 200k iterations yields on average 170(2) meV higher absolute energies than the single-point one. This highlights the improved error cancellation properties afforded by joint optimization. At the same time, the absolute energies of the transferable ansatz were still converging when the optimization was stopped, indicating the possibility of further reducing the total energy error with extended optimization.

Even with dynamic state ordering and sharing of network parameters across states, we did not succeed in keeping the continuity of the  $X^1\Sigma_g^+$  and  $A^1\Pi_u$  states at large bond lengths, where they are very nearly degenerate ( $> 1.6$  Å). However, these settings do have a beneficial effect on the continuity of the  $a^3\Pi_u$  and  $c^3\Sigma_u^+$  states at their crossing, where continuity is preserved consistently only with these settings activate.

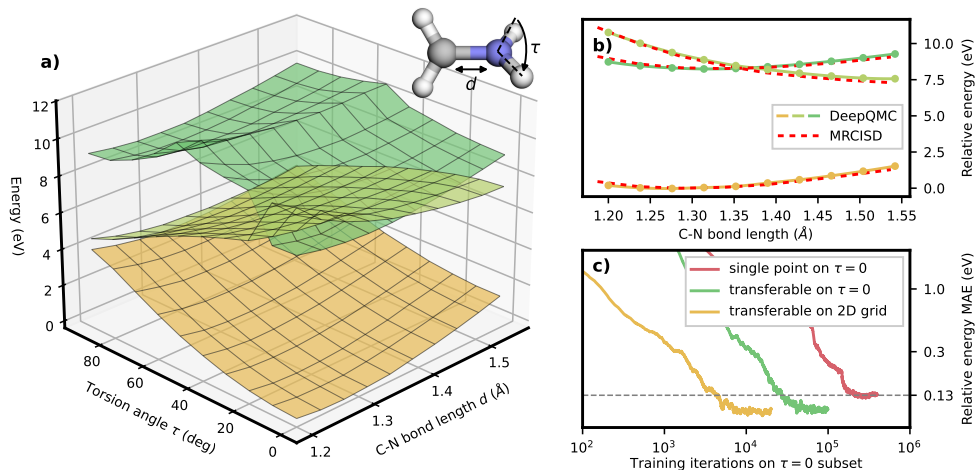


**Fig. 4 2D singlet PESs of the methyleniminium cation.** Transferable DeepQMC simulations on  $\text{CH}_2\text{NH}_2^+$  for varying C–N bond lengths (1.2–1.54 Å) and torsion angles  $\tau$  (0–90°). **a)**: Relative energies of the three lowest-lying singlet PESs of the  $\text{CH}_2\text{NH}_2^+$  on a uniform  $10 \times 10$  grid. **b)**: 1D slice of the 2D PES at  $\tau = 0$ , comparing transferable DeepQMC results with MR-CISD+Q/SA-9-CAS(6,4)/d-aug-cc-pVDZ data from Ref. [41]. **c)**: Convergence of the mean absolute error of relative energies between the three lowest-lying singlet states evaluated at ten configurations with  $\tau = 0$  (C–N bond length between 1.2–1.54 Å), using MR-CISD [41] as a reference. Single-point and two transferable neural network VMC optimizations are compared. The first transferable training was carried out on the  $10 \times 10$  grid (varying C–N and  $\tau$ ), while the second only on the 10-point subset at  $\tau = 0$ . The horizontal axis indicates the total cumulative iterations across all geometries considered, re-normalized to take into account differences in the electron batch sizes. The dashed horizontal line marks the final accuracy of the single-point simulations.

## Higher computational efficiency gains for multidimensional potential energy surfaces

We conclude by presenting results on the excited states of the methyleniminium cation,  $\text{CH}_2\text{NH}_2^+$ , the simplest model of protonated Schiff bases undergoing isomerization. As such, it is extensively studied in the context of photodynamics [41, 42], and more recently became the target of neural network force fields for excited states [43]. Following a  $\pi \rightarrow \pi^*$  excitation, the system can first relax to the first excited state via elongation of the C–N bond combined with slight bi-pyramidalization, and then to the ground state via torsional motion. Accurately capturing this relaxation remains a challenge for CASSCF, overshooting the  $\pi\pi^*$  state in the Franck–Condon region [41]. Accordingly, the more computationally expensive MR-CISD calculations are to-date the *de facto* references for the study of this system [41].

In contrast to the small scale study of ethylene and carbon dimer, we now turn to a two-dimensional problem, covering key molecular configurations relevant for the relaxation of  $\text{CH}_2\text{NH}_2^+$ . We generate a  $10 \times 10$  grid of nuclear configurations, spanning the two most relevant degrees of freedom in the problem: the torsion angle  $\tau$  and the C–N bond length. Unlike in previous examples, here we employ ccECP-type



pseudopotentials [44, 45]. While not strictly necessary, this choice speeds up convergence and reduces the memory required for storing electron position samples for each molecular configuration. We found that sharing network parameters across states did not provide a clear advantage, therefore we maintain separate parameters for each state. We believe that the use of pseudopotentials diminishes the benefits of parameter sharing, as a significant portion of the shared wave function features is lost when replacing core electrons with effective potentials.

In Fig. 4a, we present the 2D PES of the methylenimmonium cation on a uniform grid: the C–N bond length ranging from 1.2 to 1.54 Å, with torsion angles between 0° and 90°. First, the qualitative agreement across the whole grid with the MR-CISD+Q/SA-9-CAS(6,4)/d-aug-cc-pVDZ reference results from Ref. [41] is noted. Our model correctly captures the approach of the ground and first excited states with increasing torsion angle, as well as the crossing of the first and second excited-state PESs at  $\tau = 0$ . In Fig. 4b we further inspect a slice of the grid at  $\tau = 0$  and directly compare to the MR-CISD reference. Notably, dynamic state ordering enables each ansatz to follow the respective state’s character. Our results are in good agreement with Ref. [41], as the positions of the conical intersections coincide, while the remaining small differences are comparable to the accuracy of the reference method and equally plausibly may reflect its own limitations.

To assess the cost savings achieved by training jointly across molecular geometries, we compare the convergence of single-point DeepQMC calculations with two transferable models in Fig. 4c: one trained on the 100-point grid described above, the other trained only on the subset of ten molecular configurations with  $\tau = 0$ . Similar to Fig. 2b and 3b, we utilize the MAE of relative energies, computed for the ten geometries with  $\tau = 0$ , to compare the convergence of the various DeepQMC calculations. Unlike in the above studies, here the baseline single-point optimizations too were performed without supervised pretraining, facilitating a direct comparison. Once again we observe a significant convergence speedup, by roughly one order of magnitude, when going from the single-point calculations to the transferable setup with ten molecules. An additional order-of-magnitude speedup is obtained when training the transferable wave function on the larger dataset, containing 100 molecular configurations. We emphasize that the 10-point grid is a subset of the 100-point grid for a fixed torsion angle, and thus the 100-point grid covers a significantly larger section of the full PES. Finally, we highlight that transitioning to a transferable training setup not only accelerates convergence, but also improves accuracy. This is evident from the evaluated MAE (with respect to MR-CISD) dropping from the 134(2) meV of the single-point calculation to 96(2) and 97(5) meV for the 10- and 100-point transferable wave functions, respectively. Interestingly, the close agreement between the latter two suggests the robustness of our approach and raises the possibility that the discrepancy with the reference originates from its own limitations. When simulating larger parts of molecular configuration space another increasingly relevant factor is the potential for convergence to incorrect states, either due to sections that are more prone to these difficulties or simply the increasing likelihood of a few out of many single-point simulations exhibiting erroneous convergence. Here, transferable training can act as a regularizer: by correctly identifying the states for a subset of molecular configurations,

the entire transferable model is driven towards proper convergence (as observed for the second excited state of  $\text{CH}_2\text{NH}_2^+$ , see Fig. S1).

## Discussion

We have developed a computational method to simultaneously optimize the electronic wave functions and energies for ground and excited states of molecules with a range of nuclear configurations, thus obtaining *ab-initio* ground- and excited-state potential energy surfaces (PESs). This is achieved by designing a neural network wave function that is trained with quantum Monte Carlo across the desired nuclear configurations and electronic states. Due to the simultaneous representation of multiple geometries and states that is enabled by the expressivity of neural network wave functions, we obtain significant reduction of computational cost when optimizing entire PESs compared to analogous methods where each single-point calculation is done from scratch. At the same time, our approach maintains extremely high accuracy, as shown in comparison with different bespoke quantum chemistry methods that have been optimized for each considered example. The improved efficiency of joint training is demonstrated by estimating the challenging PESs of the ethylene relaxation, the carbon dimer, and the methylenimmonium cation using five, three and up to about a hundred times less compute, respectively, than the equivalent single-point DeepQMC calculations. In addition to decreased computational costs, the transferable training improves the accuracy of relative energies, as evidenced on all three test systems. The improved accuracy and stability are in large part due to the enhanced error cancellation which arises naturally if the same ansatz is used to describe all geometries in question.

An important challenge facing geometrically transferable DeepQMC based excited state methods is the presence of state crossings, where the static ordering of states in the loss function can lead to a quasi-discontinuity in the state represented by a given network. To promote the continuity of states and improve convergence, dynamic state ordering is introduced, which constructs the most appropriate loss function independently for each nuclear configuration. Furthermore, the concept of sharing large parts of the neural network parameters between models of different electronic states is introduced. If there are significant similarities between the different states, the shared parameters effectively receive more gradient information during training, contributing to the improvement over single-point results on ethylene and the carbon dimer. If, on the other hand, there is little similarity between the electronic states, for example because the highly similar core regions were replaced with effective core potentials, as is the case for the methylenimmonium cation, parameter sharing offers diminishing benefit, and can destabilize the training process.

We conclude that the presented method improves the accuracy and significantly reduces the cost of simulating excited-state PESs using deep-learning QMC approaches. Our transferable ansatz provides a coherent framework not only for accessing energies but also, as shown, for computing intermolecular overlaps across geometries (or time steps). These overlaps could be used in the surface hopping picture to approximate non-adiabatic couplings and, in turn, determine hopping probabilities [46]. At the same time, transferable simulation of excited-state PESs can be a source of

highly accurate solutions to the Schrödinger equation to be consumed in down-stream tasks, such as parameterizing excited-state force fields.

## 1 Methods

Following the time-independent Schrödinger equation:

$$\hat{H}\Psi^i = E^i\Psi^i \quad \Psi^i \in \mathcal{H}^-, \quad (3)$$

the electronic states of molecules are the eigenstates  $\Psi^i$  of the molecular Hamiltonian  $\hat{H}$ , ordered by the corresponding energy eigenvalues  $E^i$ . Additionally, electrons are subject to the fermionic anti-symmetry constraint, that is the solutions have to belong to the anti-symmetric subspace of the Hilbert space  $\mathcal{H}^-$ . To make the problem computationally tractable, in quantum chemistry, one commonly works in the Born–Oppenheimer approximation, neglecting spin-orbit coupling and other relativistic effects. For molecules this approximation is implemented by the clamped-nucleus Coulomb Hamiltonian, which in first quantization (and applying atomic units) takes the form

$$\hat{H} = \frac{1}{2} \sum_i \nabla_i^2 - \sum_{iI} \frac{Z_I}{|\mathbf{R}_{iI} - \mathbf{r}_i|} + \sum_{i<j} \frac{1}{|\mathbf{r}_i - \mathbf{r}_j|}, \quad (4)$$

with  $\nabla_i^2$  denoting the Laplace operator,  $\mathbf{r}_i$  denoting the positions of the electrons while  $Z_I$  and  $\mathbf{R}_I$  are the nuclear charges and (fixed) nuclei positions. Due to the decoupling of electronic and nuclear degrees of freedom, the Schrödinger equation holds for every molecular configuration independently, with a mere parametric dependency on the nuclei. This defines the adiabatic Born–Oppenheimer potential energy surfaces

$$\hat{H}\Psi(\mathbf{r}|\mathbf{R}) = E(\mathbf{R})\Psi(\mathbf{r}|\mathbf{R}). \quad (5)$$

### 1.1 Variational optimization

In order to approximate the eigenstates of the Schrödinger equation (3) we apply the variational Monte Carlo (VMC) method. VMC is a variational method that minimizes the Rayleigh quotient

$$\boldsymbol{\theta}' = \underset{\boldsymbol{\theta}}{\operatorname{argmin}} \frac{\langle \Psi_{\boldsymbol{\theta}} | \hat{H} | \Psi_{\boldsymbol{\theta}} \rangle}{\langle \Psi_{\boldsymbol{\theta}} | \Psi_{\boldsymbol{\theta}} \rangle} \quad (6)$$

of a parameterized trial wave function  $\Psi_{\boldsymbol{\theta}}$ . The goal is to find the optimal set of parameters  $\boldsymbol{\theta}'$ , which can then be used to evaluate expectation values. The high dimensional integrals in (6) are approximated by Monte Carlo integration with importance sampling. This stochastic integration method poses very few restriction on the functional form of the wave function ansatz, enabling the inclusion of explicit electronic correlation.

Throughout the optimization, expectation values are estimated on finite batches of electron samples drawn from the probability density associated with the square of the wave function via Markov chain Monte Carlo. At each iteration, the model parameters are updated with a flavor of stochastic gradient descent until convergence is reached.

Details on the VMC method and the peculiarities of optimizing neural network wave functions are found in earlier works [17, 45].

There are various extensions of the VMC method to target excited states. The basic requirement of these extensions is preventing the optimization from collapsing to the ground electronic state (global energy minimum), while ensuring convergence to the excited states (local energy minima). In this work we employ a penalty-based excited state optimization method [20, 47, 48], where the loss function of each state is composed of the energy of the given state plus a term penalizing its overlap with all lower-lying states. Additionally, a spin-penalty can be introduced to target states of a specific spin sector [21], leading to the complete loss function of

$$\mathcal{L}[\Psi_{\theta_1}, \dots, \Psi_{\theta_n}] = \sum_i^{N_S} \left[ \langle \hat{H} \rangle^i + \beta \langle \hat{S}^2 \rangle^i + \sum_j^{j < i} \alpha_{ij} |\langle \Psi_{\theta_i} | \bar{\Psi}_{\theta_j} \rangle|^2 \right]. \quad (7)$$

where  $\hat{S}^2$  is the total spin operator and  $\{\theta_1, \dots, \theta_n\}$  represent the parameters of the wave functions corresponding to each of the  $N_S$  different states. The bar (in  $\bar{\Psi}$ ) indicates that no gradient is taken with respect to the parameters of the specified wave function.

## 1.2 Transferable optimization

Typically, VMC is applied in the context of single-point calculations, that is the parameters of the trial wave function are optimized to minimize the energy expectation value of a specific molecular geometry. With the vastly increased expressivity of neural network wave functions, however, the concept of transferable optimization has been introduced. The idea consists of sharing a subset of the wave function parameters across multiple geometries [23] or making the ansatz explicitly dependent on the nuclear geometry [24], and minimizing the energy for multiple molecular geometries simultaneously. The transferable optimization makes use of the fact that under the Born–Oppenheimer approximation (5) the variational principle of quantum mechanics holds independently for every nuclear configuration of a molecule, that is

$$E_0(\mathbf{R}) = \min_{\Psi} \frac{\langle \Psi | \hat{H} | \Psi \rangle_{\mathbf{R}}}{\langle \Psi | \Psi \rangle_{\mathbf{R}}} \leq \min_{\theta} \frac{\langle \Psi_{\theta} | \hat{H} | \Psi_{\theta} \rangle_{\mathbf{R}}}{\langle \Psi_{\theta} | \Psi_{\theta} \rangle_{\mathbf{R}}}, \quad (8)$$

where  $\langle \dots \rangle_{\mathbf{R}}$  denotes the electronic expectation value at the nuclear geometry  $\mathbf{R}$ . In this work we combine the optimization across multiple molecular geometries (8) with the penalty based loss (7) and augment the wave function architecture to make it more suitable to the transferable setup. This yields geometrically transferable wave functions capable of describing different electronic states of a molecule across a range of molecular geometries.

We generalize the training of the wave function model by iterating through a dataset of molecular geometries  $\mathfrak{R}$ . This amounts to minimizing the average loss (7)

over the whole dataset

$$\theta' = \underset{\theta}{\operatorname{argmin}} \sum_{\mathbf{R} \in \mathfrak{R}} \mathcal{L}[\Psi_{\theta_1}, \dots, \Psi_{\theta_n}](\mathbf{R}). \quad (9)$$

In order to sample electrons for the estimation of the expectation value of the loss function at each training iteration, we employ the Metropolis algorithm and keep independent Markov chains for each geometry of the dataset in memory. To retain sufficiently large electron batches (electron batch sizes) for sufficiently accurate estimates of the expectation values, we subsample the dataset of molecules and alternate between successive batches (molecule batch size). While we find the training to be fairly insensitive to the exact choice of molecule batch size, a round robin approach with a molecule batch size of one [23] can lead to the Markov chains of other molecules going stale, especially for large datasets. Therefore, when considering larger molecule datasets, a compromise between electron batch size and molecule batch size is made (details can be found in the Supplementary Information). To account for the changes of the electron distribution due to updates of the wave function parameters, we employ a decorrelation sampler that equilibrates the Markov chains before drawing each batch of electron samples.

### 1.3 Dynamic state ordering and level crossings

The penalty based excited state optimization implements a ladder of states approach, where collapse to the ground state is prevented by orthogonalization of excited states with respect to lower-lying states (7). The resulting order of states is of no relevance in single-point simulation and the approach guarantees the optimization of pure states, as opposed to the mixed states resulting from a symmetric loss function that penalizes both ansatzes. However, when extending the loss to a transferable setting the order of the states gains importance, as the energy ordering might change at conical intersections and level crossings (right panel of Fig. 2). Albeit not strictly necessary, a continuous representation of the wave function along the geometries of the dataset is favorable both for model optimization in practice, and ease of interpreting the simulation results. To address this, we propose a more flexible penalty method where the direction of orthogonalization adapts based on relative energies at each configuration. We generalize the overlap penalty term of our loss function to be dependent on the nuclear coordinates as

$$\mathcal{L}[\Psi_{\theta_1}, \dots, \Psi_{\theta_n}](\mathbf{R}) = \dots + \sum_j^{E_{\mathbf{R}}^j < E_{\mathbf{R}}^i} \alpha_{ij} |\langle \Psi_{\theta_i} | \bar{\Psi}_{\theta_j} \rangle_{\mathbf{R}}|^2 \quad (10)$$

$$\text{where } E_{\mathbf{R}}^j < E_{\mathbf{R}}^i \implies \langle \Psi_{\theta_j} | \hat{H} | \Psi_{\theta_j} \rangle_{\mathbf{R}} < \langle \Psi_{\theta_i} | \hat{H} | \Psi_{\theta_i} \rangle_{\mathbf{R}},$$

where for simplicity we omit the sums on the configurations  $\mathbf{R}$  and on the number of states  $i$ , as they are implied. Note that the re-indexing is applied independently for every molecular configuration  $\mathbf{R} \in \mathfrak{R}$ . In practice we estimate the energy expectation values of (10) by maintaining exponential walking averages of the training energies of

each state at every geometry of the dataset. By grouping states based on their physical character, this allows the network to optimize the wave functions more effectively. While this loss does not enforce the correct ordering, we find that the continuity of the wave function is typically favored due to the smoothness of the neural network ansatz and enhanced optimization dynamics, as demonstrated on Fig. 2. The continuity of the wave functions at level crossings can be probed by evaluating intermolecular overlaps

$$O_{\mathbf{R}_m, \mathbf{R}_n}^{i,j} = \langle \Psi_{\theta_i}(\mathbf{r}, \mathbf{R}_m) | \Psi_{\theta_j}(\mathbf{r}, \mathbf{R}_n) \rangle, \quad (11)$$

between the transferable wave function of state  $i$  and  $j$  at nuclear configurations  $\mathbf{R}_m$  and  $\mathbf{R}_n$ . Fig. 2c illustrates how dynamic state ordering allows the transferable network to maintain a consistent character throughout the crossing. The overlap of the excited state wave function at  $\phi = 90^\circ$  with itself at varying  $\phi$  remains close to one, while its overlap with the ground state stays near zero. In contrast, without dynamic ordering, the network switches character at the crossing, causing the excited-state overlap to drop to zero at  $\phi = 100^\circ$  while the overlap with the ground state rises to one.

#### 1.4 Transferable ansatz

The wave function is parametrized via the usual many-body Slater-Jastrow form

$$\Psi = e^J \sum_k \det[\mathbf{A}^k], \quad (12)$$

$$A_{ij}^k = \phi_j^k(\mathbf{h}_i^{\text{elec}}) \varphi_{jk}(\mathbf{r}_i), \quad (13)$$

where  $e^J$  is a Jastrow factor,  $\phi_j^k$  are orbitals predicted from the many-body embedding of the  $i$ th electron  $\mathbf{h}_i^{\text{elec}}$ , and  $\varphi_j^k$  are envelopes of the electron coordinates  $\mathbf{r}_i$ . All reported experiments were carried out using an ansatz derived from the Psiformer architecture [31] with a few simple modifications. First, the memory bottleneck of many Psiformer-like architectures is the computation of the orbital envelope functions  $\varphi_j^k$  [27, 30]. To remedy this, we employ envelopes similar to the simplified envelopes of Gao [27], that is we compute the envelopes as

$$\varphi_j^k(\mathbf{r}_i) = \sum_I \sum_n^3 \exp(-\zeta_{Ijkn} R_{iI}). \quad (14)$$

The envelope exponents  $\zeta_{Ijkn}$  depend on the nuclear geometry, as discussed in the following. Second, while the Psiformer already receives as input the configuration of the nuclei, it only does so implicitly. Furthermore, the relative nuclear positions can influence only the electron representations  $\mathbf{h}_i^{\text{elec}}$ , while the orbital envelopes  $\varphi_j^k$  must remain fixed for all nuclear configurations. To increase our ansatz’s expressivity in representing wave functions of various nuclear geometries, we introduce a more explicit dependence on the nuclear geometry of both the electron representations and the

orbital envelopes. To this end, we compute initial embeddings for each nucleus as

$$\mathbf{h}_I^{\text{nuc},0} = \text{MLP}_{\text{embed}} \left( \sum_K^{N_{\text{nuc}}} \text{MLP}_{\text{edge}} \left( \text{Concat}(\text{OneHot}(Z_K), |\mathbf{R}_I - \mathbf{R}_K|, \mathbf{R}_I - \mathbf{R}_K) \right) \right), \quad (15)$$

where  $\mathbf{R}_I$  stands for the coordinates of nucleus  $I$ , and MLP denotes multi-layer perceptrons with a single hidden layer and SiLU activation function. The obtained initial nuclei representations are fed into the transformer blocks of Psiformer along with the embedded electrons. Causal attention is used to ensure that information flows only in one direction: from the nuclei to the electrons. The output electron representations  $\mathbf{h}^{\text{elec}}$  are then used to generate many-body orbitals just as in the original Psiformer. At the same time, from the final nucleus representations the envelope exponent parameters  $\zeta_{n,jkl}$  are predicted, by passing them through a gated linear unit [49] with sigmoid activation.

## 1.5 Sharing parameters between states

Parameter sharing has been demonstrated to be very efficient when transferably simulating ground states via exploiting similarities in the wave functions of different molecular configurations. Analogous similarities may arise when simulating multiple electronic states of a molecule, i.e. due to the presence of core orbitals, which are not involved in any of the electronic excitations. While previous works employed distinct sets of model parameters for each excited state respectively [20, 21, 50], we propose to share a large fraction of the model parameters between the states

$$\Psi_{\theta_1}(\mathbf{R}), \dots, \Psi_{\theta_n}(\mathbf{R}) \rightarrow \Psi_{(\theta_1, \theta^s)}(\mathbf{R}), \dots, \Psi_{(\theta_n, \theta^s)}(\mathbf{R}). \quad (16)$$

Supposing that there is appreciable similarity between the wave functions of different states, parameter sharing effectively increases the number of gradient steps the shared parameters receive, potentially improving the convergence and increasing the stability of the optimization. The parameter sharing is implemented by averaging a subset of the model parameters after each gradient update. While we found that sharing all parameters of the electron-nucleus transformer works well in practice, it may lead to occasional convergence to local minima due to limiting the expressivity of the ansatz for representing distinct states. This issue can be remedied by reducing the fraction of shared model parameters, i.e. sharing only the initial layers of the transformer block, or substituting parameter sharing with implicit representations of electrons, i.e. effective core potentials.

## Declarations

**Data availability.** All data used during the creation of the manuscript figures is available from the authors upon request.

**Code availability.** The code with which the DeepQMC simulations were run will be made available on GitHub (<https://github.com/deepqmc/deepqmc>) under the MIT license, upon publication of the manuscript.

**Acknowledgements.** Funding is gratefully acknowledged from Deutsche Forschungsgemeinschaft (DFG, German Research Foundation) under Germany’s Excellence Strategy – The Berlin Mathematics Research Center MATH+ (EXC-2046/1, project ID: 390685689) projects (AA1-6, AA2-8) and Deutsche Forschungsgemeinschaft (DFG, German Research Foundation) project NO825/3-2. A. Cuzzocrea acknowledges support from the Alexander von Humboldt Foundation. The authors thankfully acknowledge the computing time granted by the Resource Allocation Board and provided on the supercomputer Lise at NHR@ZIB as part of the NHR infrastructure. The calculations presented here were conducted with computing resources under the project bem00084.

**Author contributions.** ZS, PBS, AC and FN conceived the project. ZS, PBS and AC developed the method in full detail. ZS and PBS wrote the computer code with contributions from AC. The numerical experiments were conceived, carried out, and analyzed by ZS, PBS, and AC. ZS, PBS and AC wrote the manuscript with input from FN. FN supervised the project. Funding was acquired by AC and FN.

**Competing interests.** The authors declare no competing interests.

## References

- [1] Gozem, S., Luk, H.L., Schapiro, I., Olivucci, M.: Theory and Simulation of the Ultrafast Double-Bond Isomerization of Biological Chromophores. *Chemical Reviews* **117**(22), 13502–13565 <https://doi.org/10.1021/acs.chemrev.7b00177>
- [2] Curutchet, C., Mennucci, B.: Quantum Chemical Studies of Light Harvesting. *Chemical Reviews* **117**(2), 294–343 <https://doi.org/10.1021/acs.chemrev.5b00700>
- [3] Westermayr, J., Gastegger, M., Vörös, D., Panzenboeck, L., Joerg, F., González, L., Marquetand, P.: Deep learning study of tyrosine reveals that roaming can lead to photodamage. *Nature Chemistry* **14**(8), 914–919 <https://doi.org/10.1038/s41557-022-00950-z>
- [4] Risko, C., D. McGehee, M., Brédas, J.-L.: A quantum-chemical perspective into low optical-gap polymers for highly-efficient organic solar cells. *Chemical Science* **2**(7), 1200–1218 <https://doi.org/10.1039/C0SC00642D>
- [5] Shaw, M.H., Twilton, J., MacMillan, D.W.C.: Photoredox Catalysis in Organic Chemistry. *The Journal of Organic Chemistry* **81**(16), 6898–6926 <https://doi.org/10.1021/acs.joc.6b01449>
- [6] Deng, Y., Long, G., Zhang, Y., Zhao, W., Zhou, G., Feringa, B.L., Chen, J.: Photo-responsive functional materials based on light-driven molecular



- motors. *Light: Science & Applications* **13**(1), 63 <https://doi.org/10.1038/s41377-024-01391-8>
- [7] Alvarez-Lorenzo, C., Bromberg, L., Concheiro, A.: Light-sensitive Intelligent Drug Delivery Systems. *Photochemistry and Photobiology* **85**(4), 848–860 <https://doi.org/10.1111/j.1751-1097.2008.00530.x>
- [8] Serrano-Andrés, L., Merchán, M.: Quantum chemistry of the excited state: 2005 overview. *Journal of Molecular Structure: THEOCHEM* **729**(1), 99–108 <https://doi.org/10.1016/j.theochem.2005.03.020>
- [9] González, L., Lindh, R.: *Quantum Chemistry and Dynamics of Excited States: Methods and Applications*. John Wiley & Sons
- [10] Westermayr, J., Marquetand, P.: Machine learning for electronically excited states of molecules. *Chemical Reviews* **121**(16), 9873–9926 <https://doi.org/10.1021/acs.chemrev.0c00749>
- [11] Casida, M.E., Huix-Rotllant, M.: Progress in time-dependent density-functional theory. *Annual Review of Physical Chemistry* **63**, 287–323 <https://doi.org/10.1146/annurev-physchem-032511-143803>
- [12] Herbert, J.M.: Density-functional theory for electronic excited states. In: *Theoretical and Computational Photochemistry*, pp. 69–118. Elsevier. <https://doi.org/10.1016/B978-0-323-91738-4.00005-1> . <https://linkinghub.elsevier.com/retrieve/pii/B9780323917384000051>
- [13] Köhn, A., Tajti, A.: Can coupled-cluster theory treat conical intersections? *The Journal of Chemical Physics* **127**(4), 044105 <https://doi.org/10.1063/1.2755681>
- [14] Stein, C.J., Reiher, M.: Automated Selection of Active Orbital Spaces. *Journal of Chemical Theory and Computation* **12**(4), 1760–1771 <https://doi.org/10.1021/acs.jctc.6b00156>
- [15] Bensberg, M., Reiher, M.: Corresponding Active Orbital Spaces along Chemical Reaction Paths. *The Journal of Physical Chemistry Letters* **14**(8), 2112–2118 <https://doi.org/10.1021/acs.jpcllett.2c03905>
- [16] Lischka, H., Nachtigallová, D., Aquino, A.J.A., Szalay, P.G., Plasser, F., Machado, F.B.C., Barbatti, M.: Multireference Approaches for Excited States of Molecules. *Chemical Reviews* **118**(15), 7293–7361 <https://doi.org/10.1021/acs.chemrev.8b00244>
- [17] Foulkes, W.M.C., Mitas, L., Needs, R.J., Rajagopal, G.: Quantum monte carlo simulations of solids. *Reviews of Modern Physics* **73**(1), 33–83 <https://doi.org/10.1103/RevModPhys.73.33>

- [18] Lester, W.A., Mitas, L., Hammond, B.: Quantum Monte Carlo for atoms, molecules and solids. *Chemical Physics Letters* **478**(1), 1–10 <https://doi.org/10.1016/j.cplett.2009.06.095>
- [19] Feldt, J., Filippi, C.: Excited-State Calculations with Quantum Monte Carlo. In: *Quantum Chemistry and Dynamics of Excited States*, pp. 247–275. John Wiley & Sons, Ltd. <https://doi.org/10.1002/9781119417774.ch8> . <https://onlinelibrary.wiley.com/doi/abs/10.1002/9781119417774.ch8>
- [20] Entwistle, M.T., Schätzle, Z., Erdman, P.A., Hermann, J., Noé, F.: Electronic excited states in deep variational monte carlo. *Nature Communications* **14**(1), 274 <https://doi.org/10.1038/s41467-022-35534-5>
- [21] Szabó, P.B., Schätzle, Z., Entwistle, M.T., Noé, F.: An improved penalty-based excited-state variational monte carlo approach with deep-learning ansatzes. *Journal of Chemical Theory and Computation* **20**(18), 7922–7935 <https://doi.org/10.1021/acs.jctc.4c00678>
- [22] Pfau, D., Spencer, J.S., Matthews, A.G.D.G., Foulkes, W.M.C.: Ab initio solution of the many-electron schrödinger equation with deep neural networks. *Physical Review Research* **2**(3), 033429 <https://doi.org/10.1103/PhysRevResearch.2.033429>
- [23] Scherbela, M., Reisenhofer, R., Gerard, L., Marquetand, P., Grohs, P.: Solving the electronic schrödinger equation for multiple nuclear geometries with weight-sharing deep neural networks. *Nature Computational Science* **2**(5), 331–341 <https://doi.org/10.1038/s43588-022-00228-x>
- [24] Gao, N., Günnemann, S.: Ab-initio potential energy surfaces by pairing gnns with neural wave functions. In: {The Tenth International Conference on Learning Representations, {ICLR} 2022, Virtual Event, April 25-29, 2022}. OpenReview.net. <https://openreview.net/forum?id=apv504XsysP>
- [25] Scherbela, M., Gerard, L., Grohs, P.: Towards a transferable fermionic neural wavefunction for molecules. *Nature Communications* **15**(1), 120 <https://doi.org/10.1038/s41467-023-44216-9>
- [26] Gao, N., Günnemann, S.: Generalizing Neural Wave Functions. In: *Proceedings of the 40th International Conference on Machine Learning*, pp. 10708–10726. PMLR. <https://proceedings.mlr.press/v202/gao23c.html>
- [27] Gao, N., Günnemann, S.: Neural pfaffians: Solving many many-electron schrödinger equations. In: Globerson, A., Mackey, L., Belgrave, D., Fan, A., Paquet, U., Tomczak, J., Zhang, C. (eds.) *Advances in Neural Information Processing Systems*, vol. 37, pp. 125336–125369. Curran Associates, Inc. [https://proceedings.neurips.cc/paper\\_files/paper/2024/file/e2d28c3ec49945e1922943070ffd21e8-Paper-Conference.pdf](https://proceedings.neurips.cc/paper_files/paper/2024/file/e2d28c3ec49945e1922943070ffd21e8-Paper-Conference.pdf)

- [28] Rende, R., Viteritti, L.L., Becca, F., Scardicchio, A., Laio, A., Carleo, G.: Foundation Neural-Network Quantum States. <https://doi.org/10.48550/arXiv.2502.09488> . <http://arxiv.org/abs/2502.09488>
- [29] Li, R., Ye, H., Jiang, D., Wen, X., Wang, C., Li, Z., Li, X., He, D., Chen, J., Ren, W., Wang, L.: A computational framework for neural network-based variational monte carlo with forward laplacian. *Nature Machine Intelligence* **6**(2), 209–219 <https://doi.org/10.1038/s42256-024-00794-x>
- [30] Pfau, D., Axelrod, S., Sutterud, H., Glehn, I., Spencer, J.S.: Accurate computation of quantum excited states with neural networks. *Science* **385**(6711), 0137 <https://doi.org/10.1126/science.adn0137>
- [31] Glehn, I., Spencer, J.S., Pfau, D.: A self-attention ansatz for ab-initio quantum chemistry. <https://openreview.net/forum?id=xveTeHVIF7j>
- [32] Ben-Nun, M., Quenneville, J., Martínez, T.J.: Ab initio multiple spawning: photochemistry from first principles quantum molecular dynamics. *The Journal of Physical Chemistry A* **104**(22), 5161–5175 <https://doi.org/10.1021/jp994174i>
- [33] Barbatti, M., Paier, J., Lischka, H.: Photochemistry of ethylene: A multireference configuration interaction investigation of the excited-state energy surfaces. *The Journal of Chemical Physics* **121**(23), 11614–11624 <https://doi.org/10.1063/1.1807378>
- [34] Shao, Y., Head-Gordon, M., Krylov, A.I.: The spin-flip approach within time-dependent density functional theory: Theory and applications to diradicals. *The Journal of Chemical Physics* **118**(11), 4807–4818 <https://doi.org/10.1063/1.1545679>
- [35] Hermann, J., Schätzle, Z., Noé, F.: Deep-neural-network solution of the electronic schrödinger equation. *Nature Chemistry* **12**(10), 891–897 <https://doi.org/10.1038/s41557-020-0544-y>
- [36] Holmes, A.A., Umrigar, C.J., Sharma, S.: Excited states using semistochastic heat-bath configuration interaction. *The Journal of Chemical Physics* **147**(16), 164111 <https://doi.org/10.1063/1.4998614>
- [37] Wouters, S., Poelmans, W., Ayers, P.W., Van Neck, D.: CheMPS2: A free open-source spin-adapted implementation of the density matrix renormalization group for ab initio quantum chemistry. *Computer Physics Communications* **185**(6), 1501–1514 <https://doi.org/10.1016/j.cpc.2014.01.019>
- [38] Mazin, I.M., Sokolov, A.Y.: Multireference algebraic diagrammatic construction theory for excited states: Extended second-order implementation and benchmark. *Journal of Chemical Theory and Computation* **17**(10), 6152–6165 <https://doi.org/10.1021/acs.jctc.1c00684>

- [39] Su, P., Wu, J., Gu, J., Wu, W., Shaik, S., Hiberty, P.C.: Bonding conundrums in the C<sub>2</sub> molecule: A valence bond study. *Journal of Chemical Theory and Computation* **7**(1), 121–130 <https://doi.org/10.1021/ct100577v>
- [40] Bruna, P.J., Wright, J.S.: Doubly excited states of C<sub>2</sub>, C<sub>2</sub><sup>+</sup>, and C<sub>2</sub><sup>2+</sup>. *Journal of Molecular Structure: THEOCHEM* **230**, 213–218 [https://doi.org/10.1016/0166-1280\(91\)85180-F](https://doi.org/10.1016/0166-1280(91)85180-F)
- [41] Barbatti, M., Aquino, A.J.A., Lischka, H.: Ultrafast two-step process in the non-adiabatic relaxation of the CH<sub>2</sub>NH<sub>2</sub><sup>+</sup> molecule. *Molecular Physics* **104**(5–7), 1053–1060 <https://doi.org/10.1080/00268970500417945>
- [42] Li, X., Xie, Y., Hu, D., Lan, Z.: Analysis of the Geometrical Evolution in On-the-Fly Surface-Hopping Nonadiabatic Dynamics with Machine Learning Dimensionality Reduction Approaches: Classical Multidimensional Scaling and Isometric Feature Mapping. *Journal of Chemical Theory and Computation* **13**(10), 4611–4623 <https://doi.org/10.1021/acs.jctc.7b00394>
- [43] Westermayr, J., Gastegger, M., Menger, M.F.S.J., Mai, S., González, L., Marquetand, P.: Machine learning enables long time scale molecular photodynamics simulations. *Chemical Science* **10**(35), 8100–8107 <https://doi.org/10.1039/C9SC01742A>
- [44] Bennett, M.C., Melton, C.A., Annaberdiyev, A., Wang, G., Shulenburger, L., Mitas, L.: A new generation of effective core potentials for correlated calculations. *The Journal of Chemical Physics* **147**(22), 224106 <https://doi.org/10.1063/1.4995643>
- [45] Schätzle, Z., Szabó, P.B., Mezera, M., Hermann, J., Noé, F.: DeepQMC: An open-source software suite for variational optimization of deep-learning molecular wave functions. *The Journal of Chemical Physics* **159**(9), 094108 <https://doi.org/10.1063/5.0157512>
- [46] Hammes-Schiffer, S., Tully, J.C.: Proton transfer in solution: Molecular dynamics with quantum transitions. *The Journal of Chemical Physics* **101**(6), 4657–4667 <https://doi.org/10.1063/1.467455>
- [47] Pathak, S., Busemeyer, B., Rodrigues, J.N.B., Wagner, L.K.: Excited states in variational monte carlo using a penalty method. *The Journal of Chemical Physics* **154**(3), 034101 <https://doi.org/10.1063/5.0030949>
- [48] Wheeler, W.A., Kleiner, K.G., Wagner, L.K.: Ensemble variational Monte Carlo for optimization of correlated excited state wave functions. *Electronic Structure* **6**(2), 025001 <https://doi.org/10.1088/2516-1075/ad38f8>
- [49] Shazeer, N.: GLU Variants Improve Transformer. <https://doi.org/10.48550/arXiv.2002.05202> . <http://arxiv.org/abs/2002.05202>

- [50] Lu, Z., Fu, W.: Penalty and Auxiliary Wave Function Methods for Electronic Excitation in Neural Network Variational Monte Carlo. <https://doi.org/10.48550/arXiv.2311.17595> . <http://arxiv.org/abs/2311.17595>